Synthesis, crystal structure and spectroscopic studies of a new silver complex derived from [1-(3-pyridinyl) ethanone]

Sibel Celik [a], Abdullah Atılgan [b,c], Meryem Alp [b], Senay Yurdakul [b,*,1], Zeynep Demircioğlu [d], Namık Özdemir [e], Orhan Büyükgüngör [f]

[a] Vocational School of Health Services, Kırşehir Ahi Evran University, Kırşehir 40100, Turkey
[b] Department of Physics, Faculty of Science, Gazi University, Ankara, Turkey
[c] Department of Energy Systems Engineering, Faculty of Engineering and Natural Sciences, Ankara Yıldırım Beyazıt University, Ankara, Turkey
[d] Department of Physics, Faculty of Arts and Science, Sinop University, Sinop, Turkey
[e] Department of Mathematics and Science Education, Ondokuz Mayıs University, Samsun, Turkey
[f] Department of Physics, Faculty of Arts and Science, Ondokuz Mayıs University, Samsun, Turkey

ARTICLE INFO

ABSTRACT

In this work, a new silver (I) complex, $[Ag(3\text{-pye})_2(H_2O)](NO_3)$ where 3-pye=1-(3-pyridinyl) ethanone, has been synthesized and characterized by elemental analyses, FT-IR, fluorescence spectroscopy, and single X-ray crystallography. The X-ray diffraction analysis revealed that the Ag(I) complex crystallized in the monoclinic system with the *C2/c* space group. Computational studies were performed using DFT approache on the present complex to get insight into the structural parameters, spectral characteristics and electronic properties. The characterization results were found to be consistent with the proposed structure of the complex, and the DFT approach supported the experimental results. Also, Hirshfeld surface analysis was used to identify the non-covalent interactions within the crystal structure as well as to visualize the conformity of the crystal structure.

1. Introduction

Pyridinyl ethanone is a chemical compound with a pyridine ring and an ethanone group (also known as a ketone group). Pyridine derivatives are utilized as a building block or intermediate in the synthesis of various pharmaceutical compounds. They can be used to create diverse pharmacologically active molecules, including many important drugs e. g. antibacterial, anticancer etc. [1–3]. Also some pyridine derivatives have shown potential as pesticides and agrochemicals [4]. These compounds can be used to protect crops from pests, diseases, and other environmental stresses [5].

The complexation of pyridine derivatives with silver nitrate likely forms coordination compounds with potential applications in various fields, such as materials science [6], catalysis [7], and medicinal chemistry [8,9]. Some pyridine-based silver compounds exhibit luminescent properties, making them useful in optoelectronics, sensors, and lighting devices [10]. The photochemical properties of silver complexes and silver's sensitivity to light (and x-rays) make it useful for the manufacture of high-quality photographic and radiographic films [11]

and photochromic lenses [12]. Therefore, the design and synthesis of novel compounds are required. It was discovered that metal complexes possess highly promising properties [13].

Rakic et al. [14] presented the synthesis, structural characterization, and cytotoxicity of trans dichloridoplatinum (II) complexes with [methyl-3-pyridyl ketone] (3-pye). Moderate to potent antiproliferative activity on various cancer cell lines was provided within that study.

This study describes the detailed characterization of a newly synthesized silver complex of [1-(3-pyridinyl) ethanone] silver nitrate complex, namely $[Ag(3\text{-pye})_2(H_2O)](NO_3)$. For this purpose, we use the X-ray diffraction method, experimental FT-IR (in the far and mid regions) spectra. In addition, DFT calculations were conducted to optimize molecular structure. Energy diagrams of molecular orbitals, molecular electrostatic potential, and Fukui functions belonging to the complex were given. Hirshfeld surface analysis is a graphical tool for visualization and understanding of intermolecular interactions including H…H, and C…H contacts. Directions and strengths of intermolecular interactions within the molecular crystal are mapped onto Hirshfeld surfaces using the normalized contact distance (d_{norm}) which is based on

---

* Corresponding author.
  E-mail address: senayy@gazi.edu.tr (S. Yurdakul).
[1] These authors contributed equally to this work.

Table 1

Crystal data and structure refinement parameters for Ag(I) complex.

Chemical formula	[$C_{14}H_{16}AgN_3O_6$]
Color/shape	Colorless/stick
Formula weight	430.17
Crystal size (mm)	$0.800 \times 0.397 \times 0.130$
Wavelength (Å)	Mo Kα, λ = 0.71073
Temperature (K)	296(2)
Crystal system	Monoclinic
Space group	*C2/c*
Unit cell parameters	
a, b, c (Å)	5.1852(4), 16.8332(17), 18.8375(14)
α, β, γ (°)	90, 91.241(6), 90
Volume (Å³)	1643.8(2)
Z	4
Density (Mgm⁻³)	1.738
μ (mm⁻¹)	1.262
Absorption correction	Integration
T_{min}, T_{max}	0.4616; 0.8533
F_{000}	864
Diffractometer/measurement method	STOE IPDS 2/ω scan
θ range for data collection (°)	$2.42 \le \theta \le 27.583$
Index ranges	$-5 \le h \le 6, -21 \le k \le 21, -24 \le l \le 24$
Reflections collected	5670
Independent/observed reflections	1886/1423
R_{int}	0.0970
Goodness of fit on F^2	1.023
Final *R* indices [$I > 2\sigma(I)$]	$R_1 = 0.0489$, w$R_2 = 0.1385$
R indices (all data)	$R_1 = 0.0635$, w$R_2 = 0.1464$
$\Delta\rho_{max.}$, $\Delta\rho_{min.}$ (e/Å³)	0.79, −0.56

both contact distances between nearest atoms present inside and outside the surfaces [15]. In this study, Hirshfeld surface analysis was used to identify the critical interactions within the crystal structure of [Ag (3-pye)$_2$(H$_2$O)](NO$_3$) that contribute to molecular packing. Also, photoluminescence properties in solid-state as well as solvent-dependent fluorescence spectra were examined.

2. Experimental and theoretical methods

2.1. Synthesis and spectroscopic measurement

Aldrich provided silver nitrate and [1-(3-pyridinyl) ethanone], which were used without additional purification. The 3-pye ligand (1 mmol), was liquefied in 20 mL of ethanol. Following that, AgNO$_3$ (0.5 mmol) was gradually added to the first obtained solution with constant mixing at ∼70 °C. The solution was filtered and wrapped in aluminum foil to protect it from light before being left to crystallize at +4 °C because slow crystallization results in larger crystal sizes and thus higher quality. The yield of the synthesized compound was 76%. The following calculated and experimental values for C, H, and N analyses were reported: [Ag(3-pye)$_2$(H$_2$O)](NO$_3$), [C$_{14}$H$_{16}$AgN$_3$O$_6$], Anal. Calc. For: C, 38.91; H, 4.20; N, 9.72%. Found: C, 38.07; H, 3.52; N, 9.65%.

Infrared spectra of Ag(I) complex and the free ligand were observed between 4000 cm⁻¹ and 550 cm⁻¹ on a Bruker FT-IR spectrometer with ATR equipment. The Far-IR spectrum was observed between 600 and 100 cm⁻¹ on the JASCO FTIR-6800 Series system. Photoluminescence (PL) measurements were made by using the Jobin Yvon Fluorolog-550 PL system with a 50 mWHeCd laser (λ=325 nm) as an excitation light source at room temperature. The elemental analysis of the chemical complex was conducted on an Elemental vario MICRO CHNS analyzer.

2.2. X-ray crystallography

Intensity data of the Ag(I) complex were collected on a STOE IPDS-II diffractometer at room temperature using graphite-monochromated Mo Kα radiation. Data collection and cell refinement were carried out using X-AREA [16] while data reduction was applied using X-RED32. The structure was solved by a dual-space algorithm using SHELXT-2018 [17] and refined with full-matrix least-squares calculations on F^2 using SHELXL-2018 [18] implemented in the WinGX [19] program suite. All carbon-bound H atoms were inserted in idealized positions and treated using a riding model. The coordinates of the H atom of the water molecule were determined by a difference Fourier map and refined isotropically, subject to a restraint of O—H=0.82(1) Å. Atom O3 of the nitrate anion showed symmetry-imposed disorder with half-occupancy about a two-fold rotation axis passing through N2···Ag1···O1W vector, and was refined without using restraints. A molecular graphic was generated by using OLEX2 [20].

Crystallographic data have been deposited with the Cambridge Crystallographic Data center as supplementary publications no CCDC 1,985,107. The details of the data collection and structure solution are listed in Table 1.

2.3. Theoretical calculations

Density functional theory (DFT) calculations were obtained with Gaussian 09 [21], and the molecule was pictured utilizing GaussView programs [22]. This structure was optimized in the gas phase starting from the X-ray geometry. A mixed basis set, including LANL2DZ for the
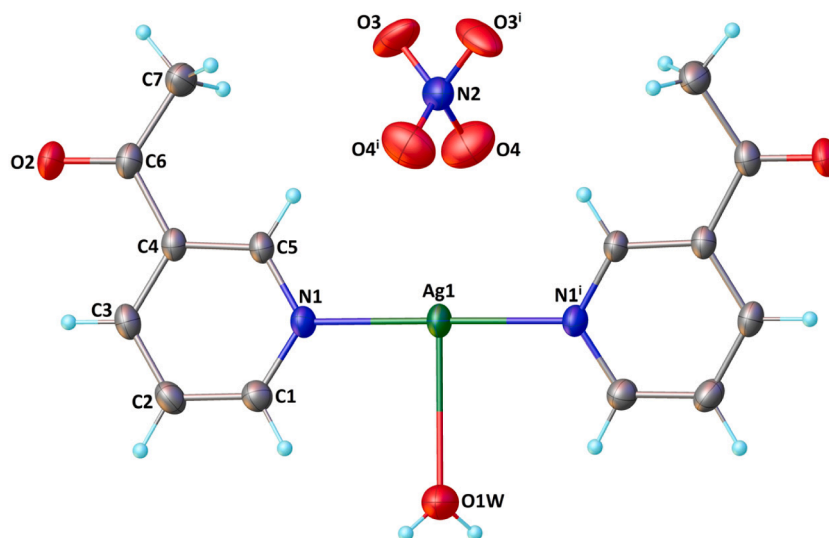
Fig. 1. Molecular structure of the Ag(I) complex [symmetry code (i): −*x* + 2, *y*, −*z* + 1/2].
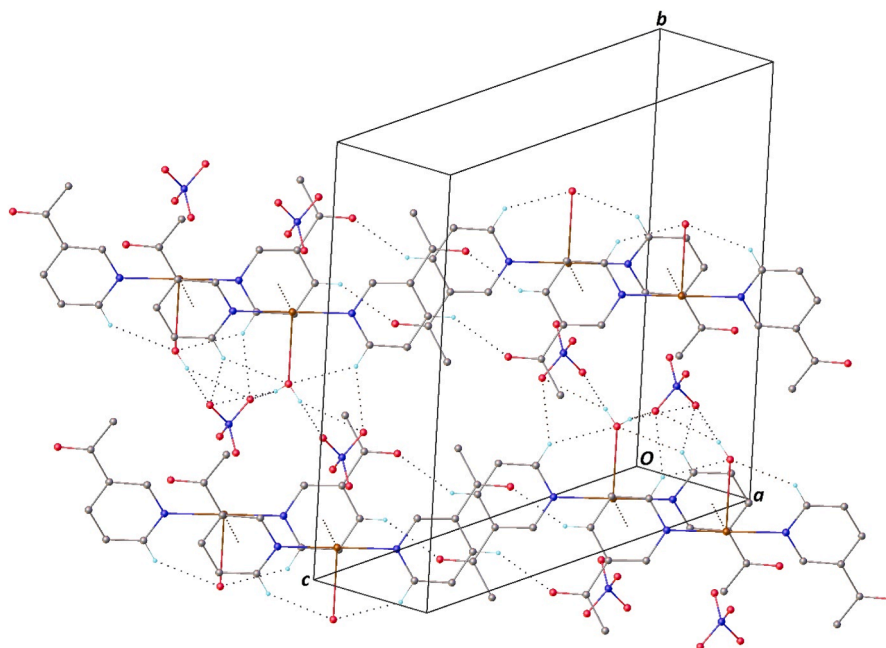
Fig. 2. Part of the crystal structure of the Ag(I) complex showing the intermolecular interactions. For the sake of clarity, H atoms not involved in the H-bonding have been omitted.

Table 2
Hydrogen bonding geometry for the Ag(I) complex.

D—H···A	D—H (Å)	H A (Å)	D···A (Å)	D—H···A (°)
O1W—H1W···O3[i]	0.83(1)	1.94(2)	2.756(12)	167(7)
O1W—H1W···O3[ii]	0.83(1)	2.58(5)	3.299(12)	146(8)
C3—H3···O2[iii]	0.93	2.56	3.364(6)	145
C1—H1···O3[iv]	0.93	2.43	3.191(9)	139
C1—H1···O1W	0.93	2.56	3.303(6)	138

Symmetry codes: [i] $x + 1/2, y + 1/2, z$
[ii] $-x + 5/2, y + 1/2, -z + 1/2$
[iii] $-x, -y + 1, -z + 1$.
[iv] $x - 1/2, y + 1/2, z$.

silver atom and 6–31G(d,p) for carbon, oxygen, nitrogen, and hydrogen atoms with B3LYP functional, was applied. The Gauss View visualization program was used to develop the molecular electrostatic potential (MEP) surface and the frontier molecular orbitals. In addition, a frontier molecular orbital analysis and a density of state analysis were performed. To support the hydrogen bonding studies, Fukui functions, and natural bond orbital (NBO) analysis were carried out. TED (Total Energy Distribution) values that were computed with the help of VEDA (Vibrational Energy Distribution Analysis) software [23–26]. The density of state spectra (DOS) were calculated using the Gauss Sum 3 software [27].
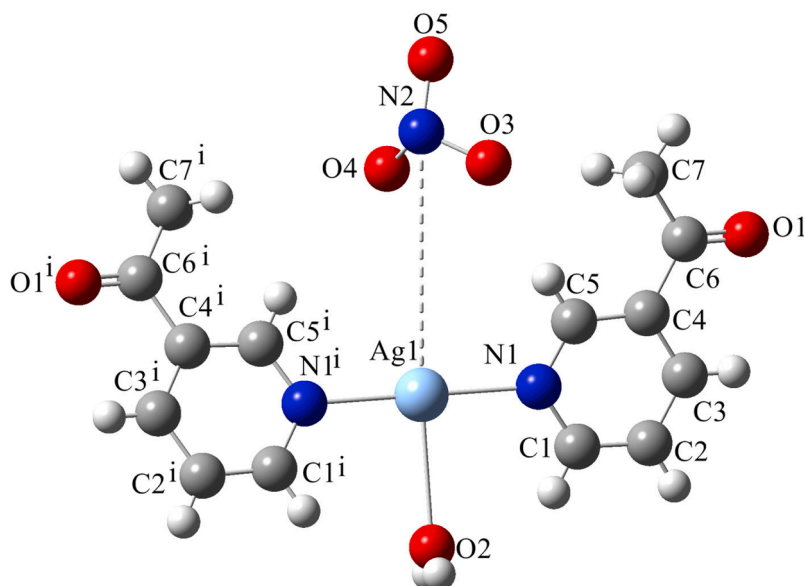

Fig. 3. Optimized molecular structure and numbering of [Ag(3-pye)$_2$(H$_2$O)](NO$_3$).

Table 3

Selected optimized geometrical parameters of Ag(I) complex obtained. Optimized geometrical parameters calculated at DFT/B3LYP/LANL2DZ (for Ag) and 6–31G(d,p) (for C,H,N,O).

Bond lengths (Å), Bond angles (°) and Torsion angles (°)	Experimental	DFT/B3LYP/LANL2DZ /6–31G(d,p)
Ag1-N1	2.178(4)	2.177
Ag1-O2W	2.767(7)	3.288
Ag1-N1[i]	2.178(4)	2.185
C5-N1	1.344(5)	1.345
C6-O2	1.210(6)	1.216
C1-N1	1.337(6)	1.362
N1-C1-C2	122.3(4)	121.6
N1-C5-C4	123.2(4)	121.5
O2-C6-C7	121.2(4)	122.5
O2-C6-C4	119.3(5)	118.3
O2W-Ag1-N1	89.77(8)	83.90
O2W-Ag1-N1[i]	89.77(8)	84.01
N1-Ag1-N1[i]	179.54(17)	181.2
C1-N1-Ag1	121.0(3)	120.9
C5-N1-C1	117.5(4)	119.3
N1-C1-C2-C3	−0.6(9)	1.02
C6-C4-C5-N1	178.9(5)	179.9
C3-C4-C5-N1	−1.0(7)	−1.25
C4-C5-N1-C1	1.4(7)	1.33
C2-C1-N1-C5	−0.6(8)	1.12
C4-C5-N1-Ag1	−174.9(4)	−178.2
C2-C1-N1-Ag1	175.8(4)	176.7

Symmetry code (i): -*x* + 2, *y*, -*z* + 1/2.
The RMSD value of complex was calculated as 0.105 for all bond distances.

3. Result and discussion

3.1. Description of the crystal structure

The Ag(I) complex crystallized in the monoclinic system and *C*2/*c* space group with *Z* = 4. The numbering scheme of this silver complex is shown in Fig.1 The asymmetric unit comprises one half of the Ag(I) ion, one [1-(3-pyridinyl) ethanone] molecule, one half of the nitrate anion, and one half the water molecule. The Ag(I) ion, the nitrogen atom of the nitrate anion, and the oxygen atom of the coordinated water molecule reside on a twofold rotation axis. The complex is three-coordinated *via* two nitrogen atoms of [1-(3-pyridinyl) ethanone] molecule and one oxygen atom of the water molecule. The Ag[I] ion is bonded to the two nitrogen atoms in an almost linear fashion with an N-Ag-N angle of 179.54(17). The oxygen atom of the aqua ligand interacts weakly with the silver atom with an Ag-O distance of 2.767(7) Å and an O-Ag-N angle of 89.77(8)°. Considering the weak Ag—O bond, the silver atom has a distorted T-shaped coordination geometry. The Ag-N distance of 2.178 (4) Å is significantly shorter than the distance of 2.285(8) Å found in [Ag (sac)(PPh3)$_2$] [28] but some of Ag-N and Ag-O distances are comparable to the corresponding bond lengths in the literature [29–34].

A ring-metal interaction with a distance of 3.428 Å between the ring centroid and silver atom is present in the crystal structure of the Ag(I) complex. The crystal structure is further stabilized by five intermolecular interactions of O—H⋯O and C—H⋯O types as shown Fig. 2, leading to the formation of a three-dimensional supramolecular network. The details of these hydrogen bonds are summarized in Table 2.

3.2. Geometry optimization

The optimized geometric structure and atomic numbering of its [Ag (3-pye)$_2$(H$_2$O)](NO$_3$) complex were presented in Fig. 3. The optimized molecular geometry of the title complex was calculated by using DFT/ B3LYP theory and functional with a mixed basis set (LANL2DZ for the silver atom and 6–31G(d,p) for carbon, oxygen, nitrogen, and hydrogen atoms). These calculations were made in the gas phase, and the initial parameters were taken from the X-ray data. The computed structural bond lengths and bond angle parameters are listed in Table 3. The parameters, which are not given in this section, are given in the supporting file (Table S1). The value of RMSD (Root Mean Square Deviation) was calculated as 0.105 for all bond distances for the title complex.

Admittedly, Ag(I) ions can form various coordination numbers and
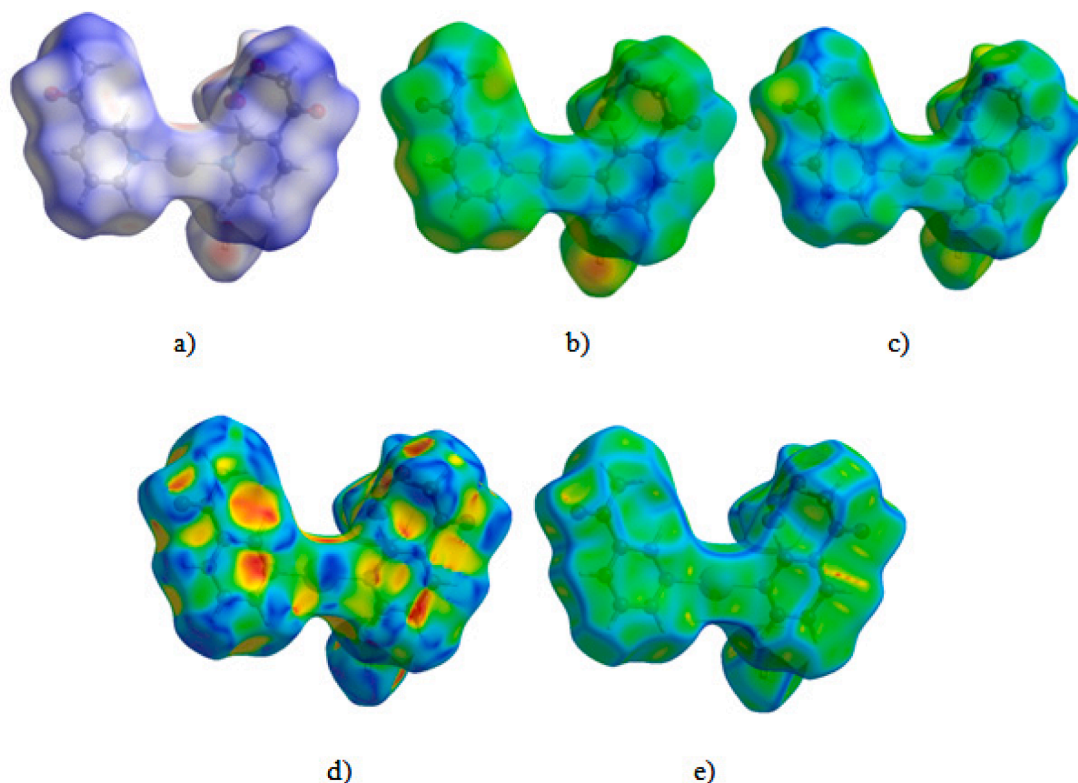
Fig. 4. Hirshfeld surface mapped with a) d$_{norm}$, b) d$_i$, c) d$_e$, d) shape index and e) curvedness for the Ag(I) complex.
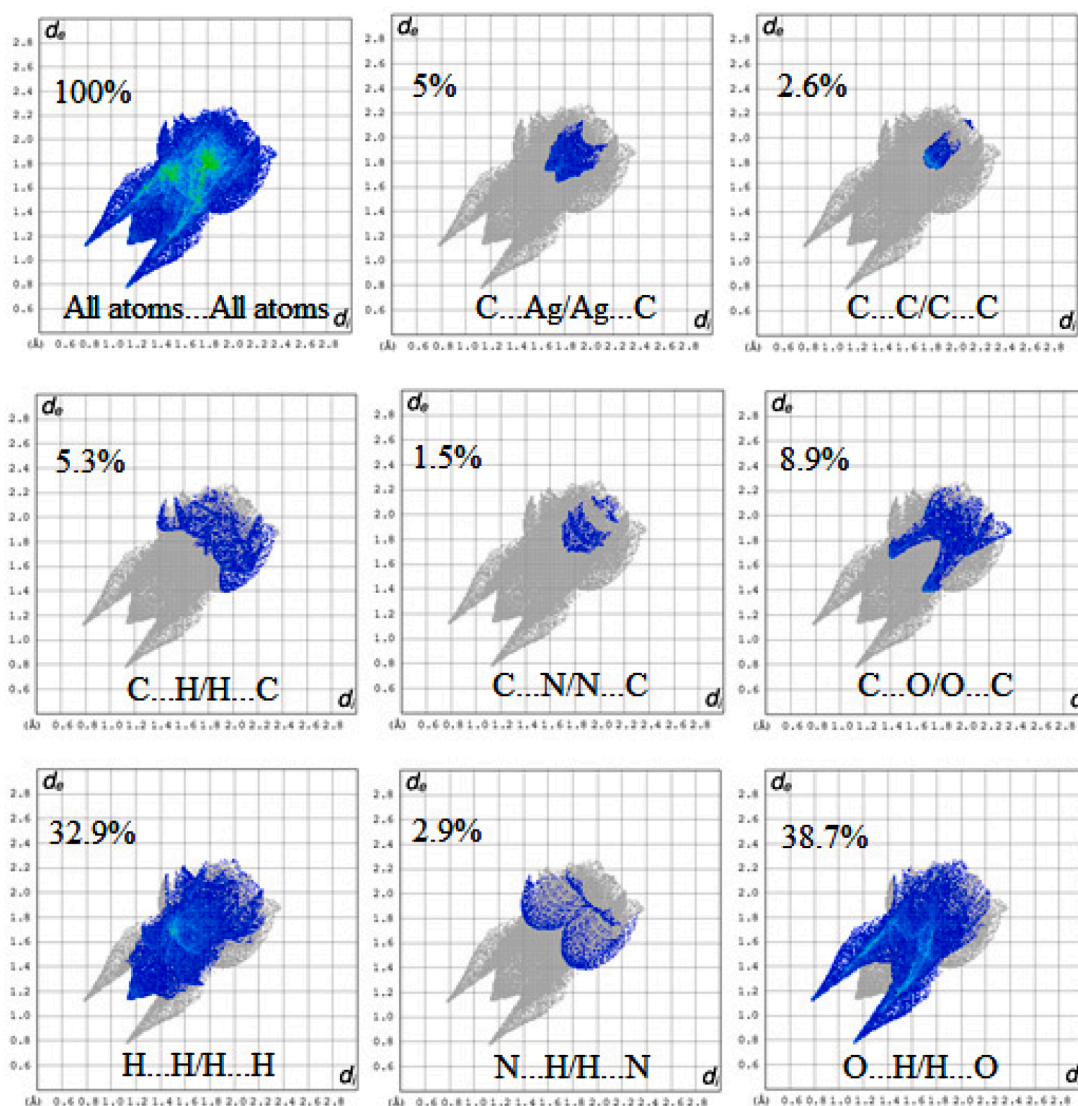
Fig. 5. Fingerprint plots of the Ag(I) complex showing interactions (d_i is the closest internal distance from a given point on the Hirshfeld surface and d_e is the closest external contacts).

geometries [35]. The present calculations have pointed out that the silver ion is coordinated to two of the ligand 3-pye and one nitrate group. The DFT method showed that the Ag-N and Ag-O bond distances are in the range of 2.24 Å (exp.: 2.18 Å) and 2.80 Å (exp.: 2.77 Å), respectively, while the calculated N-Ag-N bond angle is 181.2° (exp.: 179.54°). In comparison with the X-ray structure of the title complex, the Ag–O (exp. = 2.77(7) Å) bond distances are overestimated by about 0.03 Å. In contrast, the Ag–N bond distances appeared to be shorter (0.058 Å) than calculated. While the crystal water molecule is directly attached to the silver ion, some weak bonds were observed between the silver ion and the oxygen atom of the water molecule. Moreover, medium O—H...O interactions between the water protons and oxygen atoms of the nitrate group were observed.

The theoretical results of the geometric parameters are successfully represented by experimental data. The results, as expected, revealed some differences in the X-ray diffraction method and computational processes. According to Table 3, the comparison of results indicates that most of the computational geometrical parameters are slightly higher than the experimental values, which is attributed to the fact that computational calculations are carried out for an isolated molecule in the gas phase, while the experimental results are for the molecule in the solid state. While the NO$_3$ group was included in theoretical

calculations, the process was performed in X-ray analysis due to an unresolved disorder. The relevant explanations are given in the X-ray data solution section.

3.3. Hirshfeld surface analysis (HSA)

Hirshfeld surfaces and 2D fingerprint plots were constructed based on the electron distribution calculated as the sum of spherical atom electron densities [36]. The function d_{norm} was given by the relation involving the ratio encompassing the distances of any surface point to the nearest interior (d_i) and exterior (d_e) atoms and the van der Waals radii (r^{vdW}) of the atoms [37].

$$d_{norm} = \frac{d_i - d_i^{rdw}}{d_i^{rdw}} + \frac{d_e - d_e^{rdw}}{d_e^{rdw}} \tag{1}$$

The red regions in the Hirshfeld surfaces have negative d_{norm} values, which indicate that the sum of d_i and d_e is shorter than the sum of the relevant van der Waals radii, which is considered to be the closest contact. The white color denotes intermolecular distances close to van der Waals contacts, with d_{norm} equal to zero. The blue surfaces refer to contacts longer than the sum of van der Waals radii with positive d_{norm} values. A plot of d_i versus d_e is a 2D fingerprint plot that recognizes the

Table 4
Detailed assignments of fundamental vibrations and TED of [Ag(3-pye)$_2$(H$_2$O)](NO$_3$) complex for selected modes.

TED^c	Freq^a	I$_{IR}^b$	IR_exp	TED^c	Freq^a	I$_{IR}^b$	IR_exp
80 ν_{OH}	3779	8.2	3594 (vw)	12 Γ_{CNON}	736	0.1	
84 ν_{OH}	3662	0.4	3464 (w)	11 Γ_{ONOAg}+15 Γ_{ONOH}	720	1.0	
54 ν_{CH}	3242	3.7		20 Γ_{ONOAg}+15 Γ_{ONOH}	668	8.8	687 (m)
90 ν_{CH}	3043	0.1	3079 (w)	16 ν_{AgN}	628	3.1	
90 ν_{CH}	3034	0.3	3015 (vw)	18 δ_{CCO}	597	15.5	598 (s)
66 ν_{CO}	1660	56.8	1690 (s)	12 δ_{CCC}	477	0.4	471 (w)
18 δ_{HOH} +20 Γ_{CCOH} + 14 Γ_{NCOH}	1578	1.5	1574 (w)	10 Γ_{HCCC}	446	0.7	459 (w)
15 ν_{CC} + 30 δ_{CCH} + 30 δ_{HCH}	1437	23.0	1427 (m)	10 Γ_{HCOH}	421	0.1	414 (vw)
15 δ_{CCH} + 12 δ_{HCH}	1342	88.4	1362 (s)	16 δ_{AgCN}	365	1.0	391 (w)
25 ν_{ON} + 15 Γ_{ONOH}	1312	19.6	1321 (s)	11 δ_{CCO}	365	1.7	368 (vw)
15 ν_{CC} + 14 ν_{CN}	1306	19.5	1273 (s)	16 δ_{AgCN} + 12 δ_{HOH}	257	90.6	248 (s)
11 δ_{HCC} + 15 δ_{HCC}	1232	5.5		14 ν_{AgN} + 11 ν_{OH}	173	1.4	169 (w)
21 ν_{CH} + 15 Γ_{HCCH}	1221	100	1196 (s)	37 Γ_{CCCH} + 32 Γ_{OCCH}	159	0.5	
12 δ_{CCH} + 11 δ_{HCC}	1142	6.7		11 ν_{AgN} + 12 ν_{AgO}	137	0.5	
11 δ_{CCH}	1121	1.4	1111(w)	10 Γ_{CCCH}	125	1.5	
11 δ_{CCH}	1120	0.2		10 Γ_{CCCH}	109	0.9	
11 δ_{CCH}	1042	2.2	1048 (w)	18 ν_{OH}	108	0.4	
11 ν_{CC} + 12 ν_{CN}	1035	1.1	1030 (w)	10 Γ_{CHOH}	103	0.1	
11 Γ_{CCCH}	1023	0.1		10 Γ_{CHOH}	97	0.8	
11 Γ_{CCCH}	1009	3.4		21 ν_{OH}	80	3.1	89 (m)
12 Γ_{CCCH}	990	5.2		13 ν_{OH}	68	1.6	78 (m)
11 Γ_{CCCH}	989	2.3		13 Γ_{CNON} + 13 Γ_{ONOH}	66	1.1	67 (m)
12 Γ_{CCCH}	962	4.3	964(m)	10 ν_{OH}	56	0.3	
11 Γ_{CCCH}	864	0.3		12 Γ_{CCCC}	54	1.7	
11 Γ_{CCCH}	857	0.2	818 (w)	10 Γ_{CCCC}	48	0.1	
12 ν_{CC}	778	0.8		13 ν_{AgO}+13 Γ_{ONOH}	47	0.2	
12 Γ_{CHOH} + 11 Γ_{ONOH}	776	0.5	768 (w)	10 Γ_{CHOH}	17	0.6	

ν—stretching, δ—in-plane bending, Γ—torsion., s—strong, m—medium, w—weak, v—very, IR intensities; vs, very strong; s, strong; m, medium; w, weak; vw, very weak. ^{a}Obtained from the wave numbers calculated at B3LYP/LANL2DZ&6–31G(d,p) using scaling factors 0.9978 [43]. ^{b}Relative absorption intensities (I$_{IR}$) normalized with highest peak absorption qual to 100. ^{c}Total energy distribution (TED) less than 10% are not shown.

existence and number of different types of intermolecular interactions. The combination of d$_e$ and d$_i$ in the form of a 2D fingerprint plot [38] provides a summary of the intermolecular contacts in the crystal [39]. For Ag(I) complex, d_{norm}, d_i, d_e, *shape index, and curvedness indexes* are −1.2102 to 1.2289, 0.5905 to 2.4004, 0.6213 to 22,759, −1 to +1 and −4 and +4 Å, respectively. The maps of d_{norm}, d_i, d_e, *shape index,* and curvedness on molecular Hirshfeld surfaces are shown in Fig. 4.

The d$_i$ is the closest internal distance from a given point on the Hirshfeld surface, and d$_e$ is the closest external contact. The d$_e$ denotes the distance of any surface point nearest to the interior atom; the second factor and d$_i$ represent the distance of the surface point nearest to the exterior atom and also the Van der Waals ratio of the atom. The red regions represent that the ring carbon atoms were located outside the surface, while the blue color represents that they were located inside the surface for d$_i$ and d$_e$ Hirshfeld surfaces.

Fingerprint plots in Fig. 5 indicate the relative contributions to the Hirshfeld surface (in%) and difference between intermolecular interaction patterns. The largest portion of the total Hirshfeld surface belongs to H…H/H…H and O…H/H…O close contacts, with 32.9% and 38.7%, respectively. The other forces are C…C/C…C (2.6%), C…H/H…C (5.3%), C…N/N…C (1.5%), C…O/O…C (8.9%), C…Ag/Ag…C (5%) and N…H/H…N (2.9%) contacts for Ag(I) complex (Fig. 5). The fingerprint plots and molecular Hirshfeld surfaces are good ways to understand the contributions of various intercontacts, which help stabilize the molecular structures.

3.4. Assignment of vibrational spectra

The calculated vibrational frequencies and intensities using B3LYP/LANL2DZ for Ag and 6–31G(d,p) for (C, H, N, O) of [Ag(3-pye)$_2$(H$_2$O)](NO$_3$) were presented in Table 4. A detailed description of the normal modes of the title complex by means of TED derived from DFT calculations was tabulated in Table 4, and the experimental and theoretical infrared spectra of [Ag(3-pye)$_2$(H$_2$O)](NO$_3$) as presented in Fig 6. The

vibrational parameters, which were not given in this section, were presented in the supporting file (Table S2).

3.4.1. C-H and O-H vibrations

The Ag(I) complex has eight aromatic C-H bonds, which lead it to undergo stretching vibrations associated with the ring calculated in the range of 3242–3200 cm^{-1}. The TED contribution to these stretching modes pointed out that these are highly pure modes. Since the complex has two acetyl groups, six C-H stretching vibrations were expected. Compared to the aromatic C-H ring vibrations, these stretching vibrations obtained in the range of 3179–3034 cm^{-1}. In the current study, symmetric C-H stretching modes were observed at 3079 cm^{-1} and 3015 cm^{-1}. Asymmetric stretching modes were calculated as 3123 cm^{-1} and 3110 cm^{-1}. It is known that, asymmetric stretching modes are generally observed at a higher frequency compared to the symmetric stretching modes [34,35].

The deformation vibration of the acetyl group was observed at 1427 cm^{-1} (medium) in the case of the complex, while this mode was calculated at 1437 cm^{-1}. The characteristic region of C–H in-plane bending vibrations is expected to fall around 1420–900 cm^{-1}. Some of them calculated as 1383 cm^{-1} ,1342 cm^{-1} ,1240 cm^{-1} ,1232 cm^{-1} ,1142 cm^{-1} ,1141 cm^{-1} ,1121 cm^{-1}, 1120 cm^{-1}.

The O-H stretching vibrations of the title complex were calculated at 3779 and 3662 cm^{-1}, respectively. These vibration modes were observed at 3494 cm^{-1}, and 3464 cm^{-1} as weak bands in the FT-IR spectrum. The band of medium intensity of the H-O-H bending was also monitored at 1578 cm^{-1}. Calculated value was again observed in solid agreement with the experimental value, 1574 cm^{-1} (weak).

3.4.2. C=O and C-N vibrations

In the experimental FT-IR spectrum, the C=O stretching vibration was observed at 1684 cm^{-1} (very strong) [40] in the case of 3-pye, while for the [Ag(3-pye)$_2$(H$_2$O)](NO$_3$) complex, this mode was observed at 1690 cm^{-1} (strong), respectively. The spectral analysis shows that no
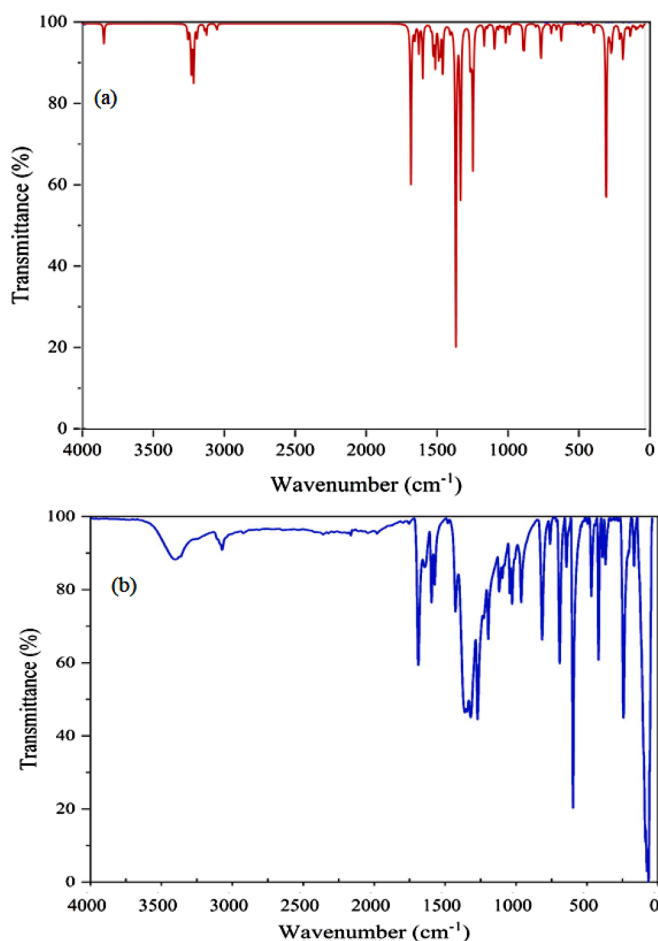
Fig. 6. FT-IR spectra of the title complex carried out theoretically (a) and experimentally (b).

significant shift is observed in the carbonyl band of the title complex. The lack of a shift in this band suggests that the ligand's carbonyl oxygen atoms are not in coordination with the metal atom in the complex. The peak at 1304 cm^{-1} [40], corresponding to υ(C=N) in the IR spectrum of the free ligand, shifts to 1273 cm^{-1} upon complexation, indicating ligand nitrogen coordination. The shift in the band due to the coordination of nitrogen with the Ag(I) ion is supported by X-ray analysis of the complex.

3.4.3. N-O stretching vibrations

The IR spectra of nitrate complexes showed the typical IR frequency for the uncoordinated nitrate group by the appearance of medium intensity in the 1375–1285 cm^{-1} range as a result of the asymmetric stretching of the nitrate group (NO$_3$) [41]. The coordination of the

nitrate ion in the complex is demonstrated by the new band seen at 1321 cm^{-1} in the spectrum of the title complex.

3.4.4. Ag-O and Ag-N stretching vibrations

Particular attention was given to the location of the Ag-N and Ag-O stretching vibrations. The compound includes two Ag-N bonds between metal and ligands. Thus, two Ag-N stretching modes were calculated at 628 cm^{-1} and 173 cm^{-1}. In the literature, these modes were measured at 450–350 cm^{-1} [41]. Ag-O peaks were calculated at 668 cm^{-1}, at 137 cm^{-1} and experimentally observed at 687 cm^{-1}. These in-plane and out-of-plane bending vibrations calculated at a lower frequency were of very low intensity. The differences between the literature and the current study can be explained by the size of the molecular structure of the title compound and the existence of many inter- and intra-molecular interactions. In particular, the aforementioned hydrogen bond affected these vibrations and caused shifts in peak positions. Among the vibrational properties of nitrate, there is an interesting case of silver-nitrate interaction. The silver atom has produced a stretching vibration with the nitrogen atom of nitrate. In this case, there seems to be stretching vibration in Ag-N. Furthermore, because the oxygen atoms of the nitrate form hydrogen bonds with the hydrogen atoms of the ligands, this mode has an O-H stretching vibration.

The relatively short Ag-N bond length (2.177(4) Å) was supported by the quite high frequencies of the Ag-N stretching vibrations and shows a strong silver-nitrogen bond in the title complex. Remarkably, in comparison with the Ag-N bond, the Ag-O bond was observed to be weaker and more ionic [42]. As derived from the X-ray analysis results, the Ag-N (2.177(4) Å) bond is shorter than the Ag-O (2.752(4) Å), which implies that the stretching frequency of Ag-N should be higher than that of Ag-O.

3.5. HOMO-LUMO analysis

The HOMO and LUMO energies of chemical compounds are important quantum mechanical parameters [44,45], and their values for the complex are tabulated in Table 5. The LUMO can be considered the innermost orbital, containing free places to accept electrons. The theoretical results emerging from B3LYP/LANL2DZ indicated that the title compound possesses the lowest HOMO energy (E_{HOMO}= 5.659 eV) and the highest LUMO energy (E_{LUMO}= 2.173 eV). The current complex has 3.49 eV band gap. For optical applications, bandgap (~4 eV) materials are more advantageous [46,47]. This low HOMO-LUMO energy gap is an indication of low stability and high chemical reactivity for the title compound. This makes it helpful for optical applications in the area.

The plots of HOMO, HOMO-1, LUMO, and LUMO+1 molecular orbitals for the complex were presented in Fig. 7. The blue colors of the MO's plot pointed out the strongest attraction, while the red colors represented the strongest thrust. The HOMO was located over silver nitrate, while the LUMO electron density was localized on the pyridine ring. The HOMO→LUMO transitions indicate the electron density will transfer from nitrate group to the pyridine ring.

The HOMO-LUMO energy gap describes the molecule's final charge

Table 5
The calculated HOMO-LUMO energy gaps and quantum chemical properties of title complex at DFT/B3LYP.

No	Molecular Orbitals	Energy (eV)		Energy gap (eV)	Ionization potential (I) (eV)	Electron affinity (A) (eV)	Global hardness (η) (eV)	Electronegativity (χ) (eV)	Chemical potential (μ_c) (eV)	Global softness (σ) (eV)$^{-1}$	Global electrophilicity (ω) (eV)
1	H	−5.66	ΔE_{H-L}	3.49	5.66	2.17	1.74	3.92	−3.92	0.57	4.40
	L	−2.17									
2	H-1	−6.67	$\Delta E_{H-1-L+1}$	4.58	6.67	2.10	2.29	4.39	−4.39	0.44	4.20
	L + 1	−2.10									
3	H-2	−6.99	$\Delta E_{H-2-L+2}$	5.50	6.99	1.49	2.75	4.24	−4.24	0.36	3.26
	L+2	−1.49									

H: HOMO, L: LUMO, $\eta = \dfrac{(I-A)}{2}$, $\mu = \dfrac{-(I+A)}{2}$, $\chi = \dfrac{(I+A)}{2}$, $\sigma = \dfrac{1}{2\eta}$, $\omega = \dfrac{\mu^2}{2\eta}$, $I = -E_{HOMO}$, $A = -E_{LUMO}$.

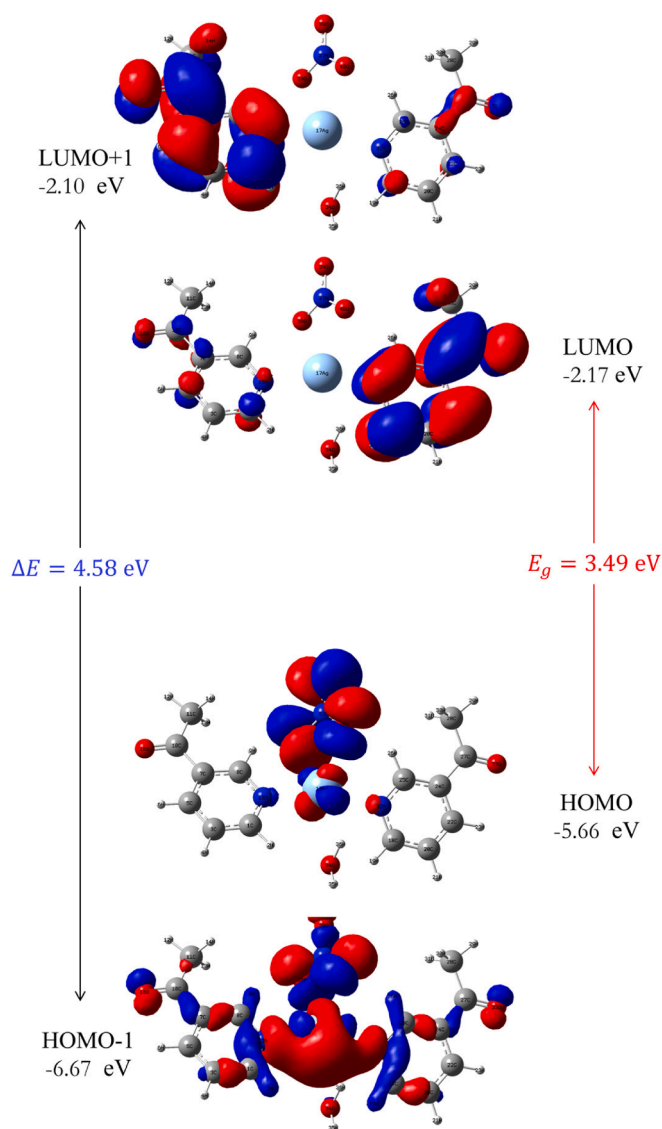**Fig. 7.** HOMO-LUMO diagram of [Ag(3-pye)$_2$(H$_2$O)](NO$_3$).

transfer interaction and may be used to calculate molecular electrical transport parameters. Calculated Molar Refractivity (MR) is a term used in quantitative structure property relationships, given as $MR=1.333\pi N\alpha$, where α is the polarizability and N is the Avogadro number [48]. For the title compounds, the MR value was observed as 79.52, and this is responsible for the binding nature of the molecular assembly and can be used for the cure of different diseases [49].

3.6. Photoluminescence properties

The fluorescence properties of metal base complexes are considered vital due to their wide range of applications in chemical sensors, photochemistry, and electroluminescent displays [50,51]. The photoluminescence (PL) study of the ligand and its Ag(I) complex was detected in the range 300–1100 nm in EtOH and solid-state at room temperature. The emission spectra of the free ligand (Fig. 8) showed bands in the visible region centered at λ_{max} = 581 nm and 569 nm in solid-state and EtOH, respectively. Since the photoluminescence behavior of a 3-pye ligand in a solvent is more favorable than that of a solid state because the fluorescence behaviors are mainly ligand-centered, whereas in the solid state they are packing dependent [50]. The emission band can be assigned to the intra-ligand $\pi\rightarrow\pi^*$
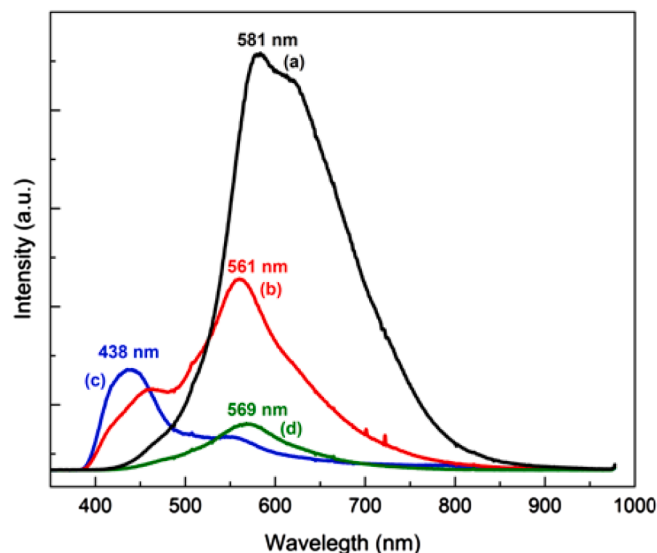

Fig. 8. Experimental Fluorescence emission spectra of (a) ligand, (b) complex in solid-state, and (c) complex in EtOH, (d) ligand in EtOH.

transition of the aromatic ring of the free ligand cation. For the complex [Ag(3-pye)$_2$(H$_2$O)](NO$_3$) the PL spectrum shows a green luminescence at 561 nm in the solid state, while the band observed in ethanol is 438 nm, which is presented in Fig. 8. The complex formation of a 3-pye ligand with Ag(I) induces a shift of the principal emission band of the ligand by 20 nm in the solid phase. The emission spectra of the compounds are ligand-centered, resulting from conjugated π-electrons, while the influence of intra-ligand charge transfer results in a double emission peak. For the obtained Ag(I) complex, both HOMO and LUMO were observed to be associated with the π-bonding orbital from the silver nitrate group, while the π^*-antibonding orbital was localized more on the pyridine rings. These characteristic emission peaks of the complex stemmed from ligand-metal charge transfer (LMCT) involving an electronic transition from a bonding nitrate orbital to a non-bonding pyridine ring orbital [52,53].

3.7. Charge analysis and Fukui functions

The electric charges of the molecule give us information about its bonding capability. Charge values have been calculated with three different approaches (NBO, APT, and Hirshfeld) by the B3LYP functional LANL2DZ basis set. In NBO analysis, orbitals are orthogonalized and localized to form one or two center orbitals. These orbitals are classified as core orbitals. Hirshfeld atomic charge analysis is based on electron density; each atom's charge is obtained by integrating the electron density over its volume. APT analysis is defined using the atomic polar tensor of the dipole moment of a molecule [54]. The calculated charge values are tabulated in Table 6 and presented in Fig. 9. The negative charge values observed in C$_2$, C$_3$, C$_4$, C$_7$, N$_1$, O$_2$, C$_2^i$, C$_{3b}^i$, C$_4^i$, C$_7^i$, N$_1^i$, O$_2^i$, O$_1$, O$_{3a}$, O$_4$, and O$_{4i}$ the most negative atoms are oxygen and pyridinic nitrogen of the complex. This indicates that during a reaction, these atoms will be preferred for binding. The positive charge values observed in C$_1$, C$_5$, C$_6$, H$_1$, H$_2$, H$_3$, H$_4$, H$_9$, H$_6$, H$_7$, Ag$_1$, C$_1^i$, H$_1^i$, H$_2^i$, H$_3^i$, C$_5^i$, H$_4^i$, C$_6^i$, H$_5^i$, H$_6^i$, H$_7^i$, H$_8$, H$_9$, and N$_2$.

Fukui functions are evaluated based on the finite-difference (FD) methodology for the molecule for neutral, cationic, and anionic charge values of optimized molecular geometry.

The Fukui functions are calculated by the following equations [55]:

$$f^+ = q_k(N+1) - q_k(N) \text{ for nucleophilic attack} \qquad (2)$$

$$f^- = q_k(N) - q_k(N-1) \text{ for electrophilic attack} \qquad (3)$$

Table 6

Comparison of APT, NBO and Hirshfeld atomic charges for [Ag(3-pye)$_2$(H$_2$O)](NO$_3$).

Atoms	APT	NBO	Hirshfeld	Atoms	APT	NBO	Hirshfeld
C$_1$	0.128	0.093	0.035	H$_2^i$	0.045	0.232	0.060
H$_1$	0.145	0.239	0.042	C$_3^i$	0.087	−0.131	−0.004
C$_2$	−0.167	−0.249	−0.044	H$_3^i$	0.101	0.251	0.068
H$_2$	0.045	0.232	0.060	C$_4^i$	−0.316	−0.166	−0.023
C$_3$	0.087	−0.131	−0.004	C$_5^i$	0.092	0.112	0.046
H$_3$	0.101	0.251	0.068	H$_4^i$	0.203	0.256	0.050
C$_4$	−0.316	−0.166	−0.023	C$_6^i$	0.906	0.577	0.162
C$_5$	0.092	0.113	0.046	C$_7^i$	−0.144	−0.722	−0.082
H$_4$	0.203	0.256	0.050	H$_5^i$	0.028	0.250	0.053
C$_6$	0.906	0.577	0.162	H$_6^i$	0.057	0.250	0.060
C$_7$	−0.144	−0.722	−0.082	H$_7^i$	0.050	0.248	0.058
H$_5$	0.028	0.250	0.053	N$_1^i$	−0.416	−0.591	−0.133
H$_6$	0.058	0.250	0.060	O$_2^i$	−0.699	−0.568	−0.264
H$_7$	0.050	0.248	0.058	O$_1$	−0.628	−0.981	−0.273
N$_1$	−0.415	−0.591	−0.133	H$_8$	0.298	0.500	0.186
O$_2$	−0.699	−0.568	−0.264	H$_9$	0.298	0.500	0.186
Ag$_1$	0.812	0.671	0.408	N$_2$	1.362	0.694	0.244
C$_1^i$	0.128	0.093	0.035	O$_3$	−0.678	−0.410	−0.276
H$_1^i$	0.145	0.239	0.042	O$_4$	−0.833	−0.568	−0.322
C$_2^i$	−0.167	−0.249	−0.044	O$_4^i$	−0.834	−0.569	−0.322
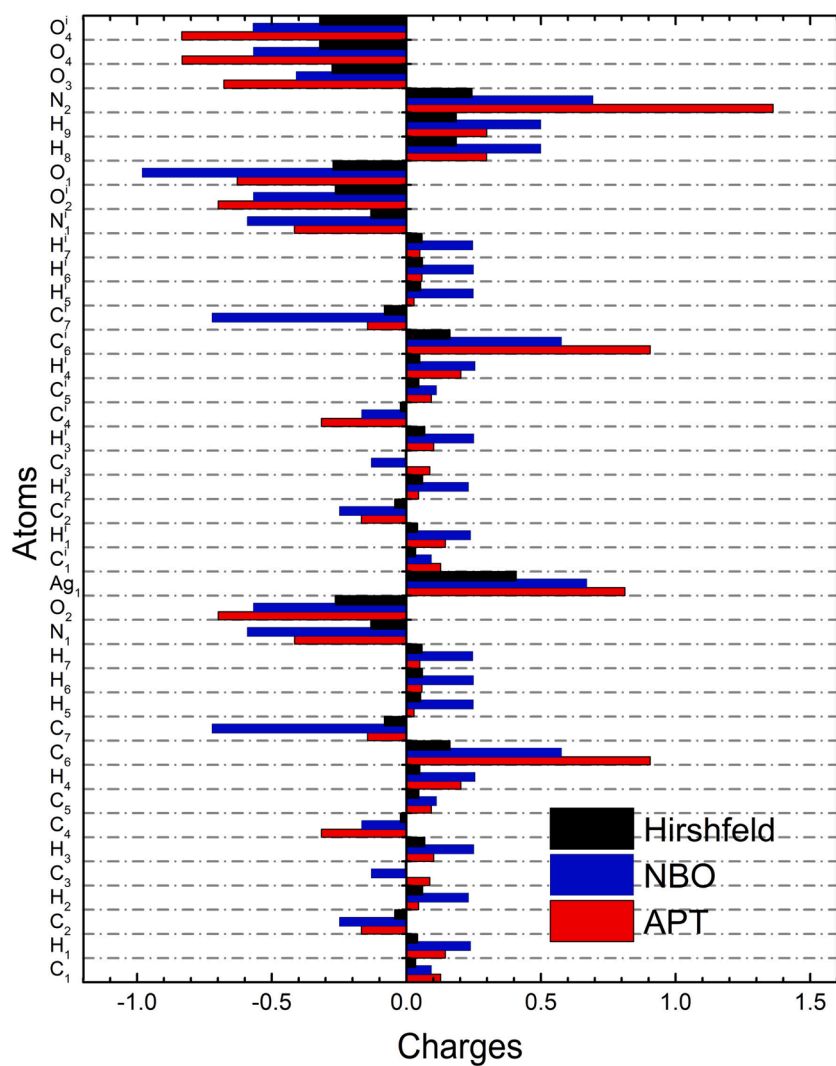
Fig. 9. Charge distribution for [Ag(3-pye)$_2$(H$_2$O)](NO$_3$).

Table 7
Condensed Fukui functions calculated from Hirshfeld charges for [Ag(3-pye)$_2$(H$_2$O)](NO$_3$).

Atoms	f^+	f^-	f^0	f^+/f^-	f^-/f^+
C$_1$	0.015	0.057	0.036	0.267	3.746
H$_1$	0.008	0.019	0.013	0.432	2.313
C$_2$	0.023	0.030	0.027	0.763	1.310
H$_2$	0.016	0.020	0.018	0.801	1.249
C$_3$	0.021	0.051	0.036	0.424	2.358
H$_3$	0.014	0.023	0.018	0.595	1.680
C$_4$	0.012	0.033	0.022	0.351	2.849
C$_5$	0.001	0.021	0.011	0.063	15.877
C$_6$	0.021	0.053	0.037	0.394	2.541
C$_7$	0.013	0.015	0.014	0.821	1.217
H$_5$	0.014	0.017	0.015	0.860	1.163
H$_6$	0.004	0.013	0.009	0.319	3.136
H$_7$	0.005	0.014	0.009	0.355	2.813
N$_1$	0.002	0.021	0.012	0.111	9.043
O$_2$	0.073	0.073	0.073	0.998	1.002
Ag$_1$	0.108	0.024	0.066	4.460	0.224
C$_1^i$	0.015	0.057	0.036	0.270	3.706
H$_1^i$	0.008	0.019	0.014	0.439	2.280
C$_2^i$	0.023	0.030	0.027	0.767	1.303
H$_2^i$	0.016	0.020	0.018	0.804	1.243
C$_3^i$	0.022	0.051	0.036	0.426	2.345
H$_3^i$	0.014	0.023	0.018	0.599	1.671
C$_4^i$	0.012	0.033	0.022	0.354	2.823
C$_5^i$	0.001	0.021	0.011	0.069	14.397
H$_4^i$	−0.002	0.010	0.004	−0.237	−4.212
C$_6^i$	0.021	0.053	0.037	0.393	2.545
C$_7^i$	0.013	0.015	0.014	0.819	1.221
H$_5^i$	0.014	0.017	0.015	0.861	1.162
H$_6^i$	0.004	0.013	0.009	0.317	3.151
H$_7^i$	0.005	0.014	0.009	0.354	2.827
N$_1^i$	0.003	0.021	0.012	0.142	7.057
O$_2^i$	0.073	0.073	0.073	0.996	1.004
O$_1$	−0.003	−0.003	−0.003	1.048	0.954
H$_8$	0.006	0.007	0.006	0.881	1.135
H$_9$	0.006	0.007	0.006	0.879	1.138
N$_2$	0.034	0.005	0.020	7.465	0.134
O$_3$	0.135	0.030	0.083	4.524	0.221
O$_4$	0.116	−0.003	0.056	−33.621	−0.030
O$_4^i$	0.117	−0.004	0.057	−33.025	−0.030

$$f^0 = (1 / 2)\ [\ q_k(N+1) - q_k(N-1)\ ]\ \text{ for neutral (radical) attack} \quad (4)$$

In these equations, q_k represents the atomic charges, and (N), (N-1), $(N+1)$ are the neutral, cationic, and anionic species of the molecule. The highest value of the (f^+/f^-) ratio is relative electrophilicity, and the highest value of the (f^+/f^-) ratio is relative nucleophilicity [56]. The data for the Fukui functions is listed in Table 7. The highest value of

electrophilic reactivity was observed at the N$_2$ atom and nucleophilic reactivity at the C$_5$ atom.

3.8. Molecular electrostatic potential maps (MEP) and density of states (DOS)

The molecular electrostatic potential (MEP) explains the electronic density distribution of molecules and presents information regarding electrophilic and nucleophilic attacks as well as hydrogen bonding interactions [57,58]. The molecular electrostatic potential (MEP) is efficiently used for detecting the presence of intra- and intermolecular interactions on the various atomic sites [34]. The negative electrostatic potential correlates to an attraction of the proton by the aggregated electron density in the molecule (shades of red), while the positive electrostatic potential correlates to a repulsion of the proton by the atomic nuclei (shades of blue). The negative (red and yellow) regions of MEP were affiliated with electrophilic reactivity and the positive (blue) regions with nucleophilic reactivity [59,60].

Figs. 10 and 11 depict the molecular electrostatic potentials (MEPs) of the [Ag(3-pye)$_2$(H$_2$O)](NO$_3$) complex. Most of the negative potentials (red color) appear to be distributed on the nitrate group and C = O, while the positive potentials (blue color) gather on water. The coordination of the silver ion with the pyridine ring through the N-atom shifts the electrostatic potential to more positive values. On the other hand, the C—H···O interactions expanded the electrostatic potential to more negative values. The MEP and the electron densities of complexes were detected in the ranges -5×10^{-2} and $+5\times10^{-2}$, respectively. It is anticipated that the most preferred region for electrophilic and nucleophilic attacks will be around nitrate and carboxyl groups, respectively.

The density of state (DOS) diagram of the title compound is given in Fig. 12. The density of states is used to indicate the number of available states of the molecular orbitals at different energies of the molecule. The DOS spectrum was calculated by Mulliken charge analysis [61]. Spectrum allows us to see more clearly occupied and virtual orbitals, respectively (green and blue lines).

4. Conclusion

A new compound [Ag(3-pye)$_2$(H$_2$O)](NO$_3$) was synthesized and characterized by experimental, theoretical, and structural (XRD) techniques. The X-ray crystal data revealed that the Ag(I) complex crystallizes in the monoclinic system with the C2/c space group. The Ag(I) ion forms a distorted T-shaped AgN$_2$O motif with an N1-Ag-N1^i angle of 179.54(17)°. The molecular geometry has been obtained by using the DFT method using the B3LYP functional and LANL2DZ, 6–31G(d, p)
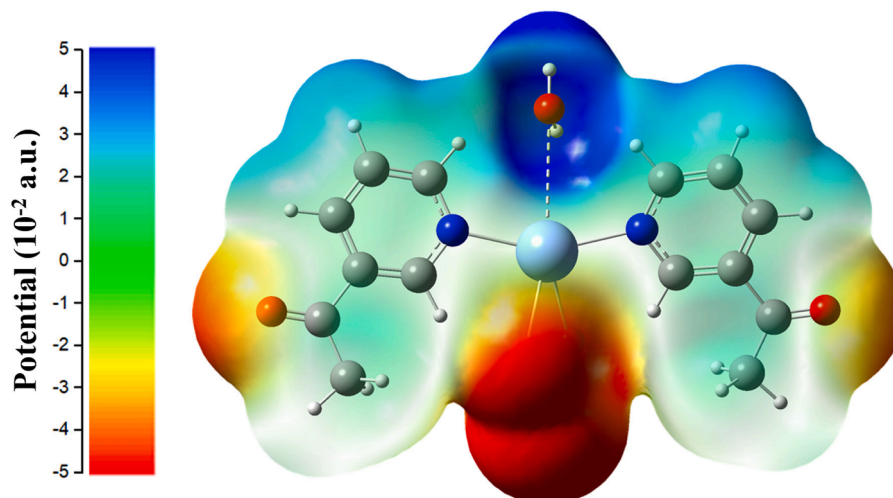

Fig. 10. Molecular electrostatic potential surface (MEP) for [Ag(3-pye)$_2$(H$_2$O)](NO$_3$).
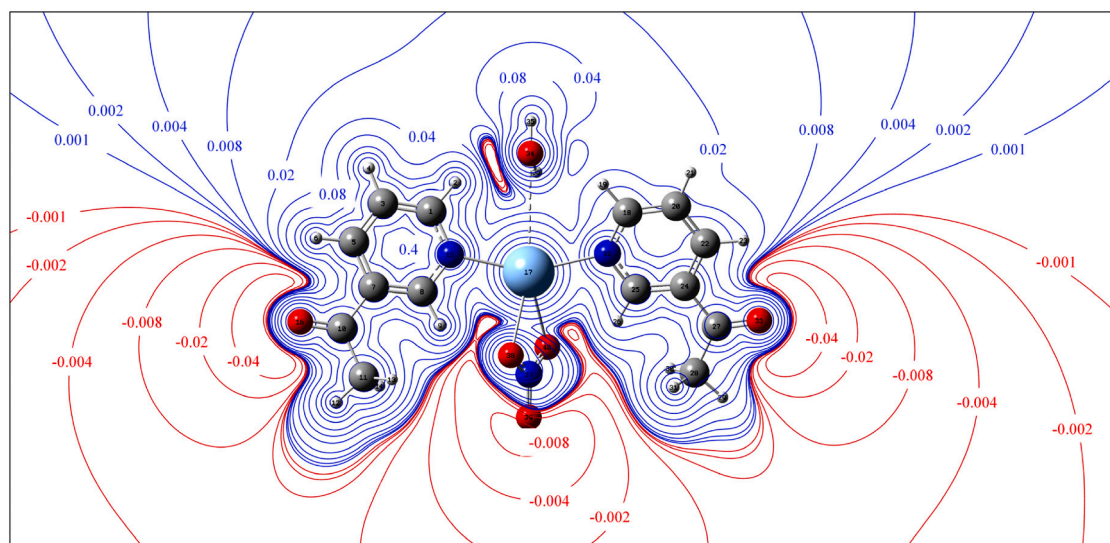
Fig. 11. 2D contour map of Molecular electrostatic potential surface (MEP) for [Ag(3-pye)$_2$(H$_2$O)](NO$_3$).
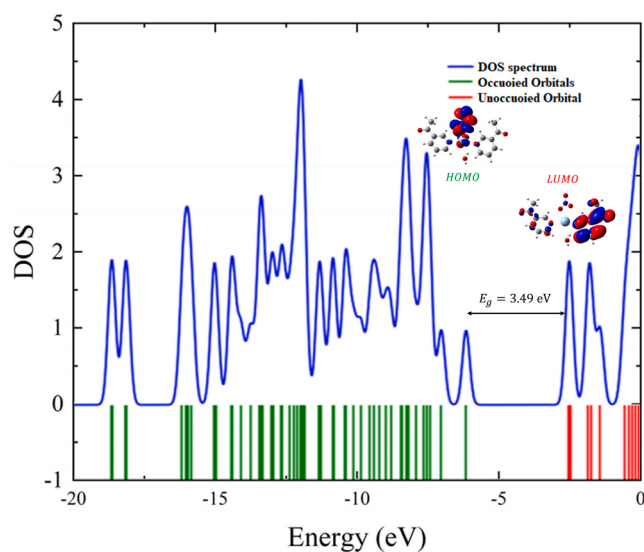
Fig. 12. DOS Spectrum of [Ag(3-pye)$_2$(H$_2$O)](NO$_3$).

mixed basis set.

In this study, comparisons between the computed and experimental geometric parameters and vibrational frequencies have been reported and discussed. The experimental results were seen to adapt to the theoretical ones. The molecular electrostatic potential (MEP) plot for the title compound shows that the negative charges are around the nitrate group and C=O, while the positive charges appear at the water molecule. The HOMO-LUMO energy gap was calculated to be 3.49 eV. That is to say, this molecule has low stability and can show optical properties. The [Ag(3-pye)$_2$(H$_2$O)](NO$_3$) complex also showed remarkable luminescence in the solid-state photoluminescence spectrum.

Ethical approval

Authors declare that ethical issues are considered and ensured throughout the study process.

Consent to participate

All authors declare their consent to participate into the study.

Consent to publish

All authors declare their consent to publish the manuscript.

Availability of data and materials

Authors declare that all data and materials are preserved properly and to be shared in case needed.

Supplementary Material

Crystallographic data for the compound reported in this article has been deposited with the Cambridge Crystallographic Data center, CCDC No. 1,985,107. These data can be obtained free of charge from The Cambridge Crystallographic Data center *via* https://www.ccdc.cam.ac.uk/structures.

CRediT authorship contribution statement

Sibel Celik: Data curation, Software. **Abdullah Atılgan:** Software. **Meryem Alp:** Software, Visualization, Data curation, Writing – review & editing. **Senay Yurdakul:** Supervision, Conceptualization, Writing – review & editing. **Zeynep Demircioğlu:** Formal analysis. **Namık Özdemir:** Formal analysis. **Orhan Büyükgüngör:** Formal analysis.

Declaration of Competing Interest

The authors declare that they have no known competing financial interests or personal relationships that could have appeared to influence the work reported in this paper.

Data availability

The authors do not have permission to share data.

Supplementary materials

Supplementary material associated with this article can be found, in the online version, at doi:10.1016/j.molstruc.2023.136468.

References

[1] S.R. Alizadeh, M.A. Ebrahimzadeh, Antiviral activities of pyridine fused and pyridine containing heterocycles, Min. Rev. Med. Chem. 21 (17) (2021) 2584–2611.

[2] D.K. Lang, R. Kaur, R. Arora, B. Saini, S. Arora, Nitrogen-containing heterocycles as anticancer agents: an overview, anti-cancer agents, Medicin. Chem. 20 (18) (2020) 2150–2168.

[3] J.C. Liu, S. Narva, K. Zhou, W. Zhang, A review on the antitumor activity of various nitrogenous-based heterocyclic compounds as NSCLC inhibitors, Mini Rev. Med. Chem. 19 (18) (2019) 1517–1530.

[4] A.Y. Guan, C.L. Liu, X.F. Sun, Y. Xie, M.A. Wang, Discovery of pyridine-based agrochemicals by using intermediate derivatization methods, Bioorg. Med. Chem. 24 (3) (2016) 342–353.

[5] A. Burriss, A. Edmunds, D. Emery, R. Hall, O. Jacob, J. Schaetzer, The importance of trifluoromethyl pyridines in crop protection, Pest Manag. Sci. 74 (6) (2018) 1228–1238.

[6] H.Y. Yang, K.Y. He, X. Ai, X. Liu, Y. Yang, S.B. Yin, P.J. Jina, Y. Chen, Pyridine functionalized silver nanosheets for nitrate electroreduction, J. Mater. Chem. A 30 (2023) 16068–16073.

[7] M. Trose, M. Dell'Acqua, T. Pedrazzini, V. Pirovano, E. Gallo, E. Rossi, A. Caselli, G. Abbiati, [Silver(I)(pyridine-containing ligand)] complexes as unusual catalysts for A3-coupling reactions, J. Org. Chem. 79 (16) (2014) 7311–7320.

[8] K.A. Ali, M.M. Abd-Elzaher, K. Mahmoud, Synthesis and anticancer properties of silver(I) complexes containing 2,6-Bis(substituted)pyridine derivatives, Int. J. Med. Chem. 2013 (2013) 256836.

[9] M.A. El-Naggar, M.A.M. Abu-Youssef, S.M. Soliman, M. Haukka, A.M. Al-Majid, A. Barakat, A.M.A. Badr, Synthesis, X-ray structure, Hirshfeld, and antimicrobial studies of new Ag(I) complexes based on pyridine-type ligands, J. Mol. Struct. 1264 (2022), 133210.

[10] G. Colombo, G.A. Ardizzoia, S. Brenna, Imidazo[1,5-a]pyridine-based derivatives as highly fluorescent dyes, Inorg. Chim. Acta 535 (2022), 120849.

[11] F.H. Mohammed, A.A.H. Abdel-Rahman, M.A. Hawata, R. El Araby, E. Guibal, A. Fouda, Y. Wei, N.A. Hamad, Functionalization of magnetic chitosan microparticles – comparison of trione and trithione grafting for enhanced silver sorption and application to metal recovery from waste X-ray photographic films, J. Environ. Chem. Eng. 10 (3) (2022), 107939.

[12] I.R. Gould, J.R. Lenhard, A.A. Muenter, S.A. Godleski, S.Y. Farid, New approach to silver halide photography using radical cation chemistry, Pure Appl.Chem 73 (3) (2001) 455–458.

[13] S.Ünlü Hezam, F. Tuncel Elmalı, Metal complexes derived from tetradentate Schiff base ligands: synthesis, spectroscopic analysis, thermogravimetric degradation and antimicrobial activities, J.Mol. Struct. 1293 (2023), 136156.

[14] G.M. Rakić, S. Grgurić-Šipka, G.N. Kaluđerović, S. Gómez-Ruiz, S.K. Bjelogrlić, S. Radulović, Z.L. Tešić, Novel trans-dichloridoplatinum (II) complexes with 3-and 4-acetylpyridine: synthesis, characterization, DFT calculations and cytotoxicity, Eur. J. Med. Chem. 44 (5) (2009) 1921–1925.

[15] S. BelhajSalah, Mohammed S.M. Abdelbaky, Santiago García-Granda, K. Essalah, C. Ben Nasr, M.L. Mrad, Crystal structure, Hirshfeld surfaces computational study and physicochemical characterization of the hybrid material (C7H10N)2[SnCl6]·H2O, J. Mol. Struct. 1152 (2018) 276–286.

[16] X. Stoe&Cie, AREA (Version 1.18) and X-RED32 (Version1. 04), Stoe&Cie, Darmstadt, Germany, 2002.

[17] G.M. Sheldrick, SHELXT–integrated space-group and crystal-structure determination, Acta Cryst. Sec. A Found. Adv. 71 (1) (2015) 3–8.

[18] G.M. Sheldrick, Crystal structure refinement with SHELXL, Acta Cryst. Sec. C Struc. Chem. 71 (1) (2015) 3–8.

[19] L.J. Farrugia, WinGX and ORTEP for Windows: an update, J. Appl. Cryst. 45 (4) (2012) 849–854.

[20] O.V. Dolomanov, L.J. Bourhis, R.J. Gildea, J.A.K. Howard, H. Puschmann, OLEX2: a complete structure solution, refinement and analysis program, J. Appl. Cryst. 42 (2) (2009) 339–341.

[21] M.J. Frisch, G.W. Trucks, H.B. Schlegel, G.E. Scuseria, M.A. Robb, J.R. Cheeseman, G. Scalmani, V. Barone, B. Mennucci, G.A. Petersson, H. Nakatsuji, M. Caricato, X. Li, H.P. Hratchian, A.F. Izmaylov, J. Bloino, G. Zheng, J.L. Sonnenberg, M. Hada, M. Ehara, K. Toyota, R. Fukuda, J. Hasegawa, M. Ishida, T. Nakajima, Y. Honda, O. Kitao, H. Nakai, T. Vreven, J.A. Montgomery Jr, J.E. Peralta, F. Ogliaro, M. Bearpark, J.J. Heyd, E. Brothers, K.N. Kudin, V.N. Staroverov, R. Kobayashi, J. Normand, K. Raghavachari, A. Rendell, J.C. Burant, S.S. Iyengar, J. Tomasi, M. Cossi, N. Rega, J.M. Millam, M. Klene, J.E. Knox, J.B. Cross, V. Bakken, C. Adamo, J. Jaramillo, R. Gomperts, R.E. Stratmann, O. Yazyev, A.J. Austin, R. Cammi, C. Pomelli, J.W. Ochterski, R.L. Martin, K. Morokuma, V.G. Zakrzewski, G.A. Voth, P. Salvador, J.J. Dannenberg, S. Dapprich, A.D. Daniels, O. Farkas, J. B. Foresman, J.V. Ortiz, J. Cioslowski, D.J. Fox. Gaussian 09, Gaussian, Inc, Wallingford CT, 2009.

[22] R. Dennington, T. Keith, J. Millam, GaussView, Version 5, Semichem Inc., Shawnee Mission, KS, 2009.

[23] (a) A.D. Becke, Density-functional thermochemistry. III. The role of exact exchange, J. Chem. Phys. 98 (1993) 5648;

(b) C. Lee, W. Yang, R.G. Parr, Development of the Colle-Salvetti correlation-energy formula into a functional of the electron density, Phys. Rev. B 37 (2) (1988) 785.

[24] P. Udhayakala, T.V. Rajendiran, S. Seshadri, S. Gunasekaran, Quantum chemical vibrational study, molecular property and HOMO-LUMO energies of 3-bromoace-tophenone for Pharmaceutical application, J. Chem. Pharm. Res. 3 (3) (2011) 610–625.

[25] (a) P.J. Hay, W.R. Wadt, Ab initio effective core potentials for molecular calculations. Potentials for the transition metal atoms Sc to Hg, J. Chem. Phys. 82 (1) (1985) 270–283;

(b) W.R. Wadt, P.J. Hay, Ab initio effective core potentials for molecular calculations. potentials for main group elements Na to Bi, J. Chem. Phys. 82 (1) (1985) 284–298;

(c) P.J. Hay, W.R. Wadt, Ab initio effective core potentials for molecular calculations. potentials for potassium to gold including the outermost core orbitals, J. Chem. Phys. 82 (1) (1985) 299–310.

[26] M.H. Jamroz, Vibrational Energy Distribution Analysis, 4, VEDA, Warsaw, 2010, 2004-.

[27] N.M. O'Boyle, A.L. Tenderholt, K.M. Langner, A library for package independent computational chemistry algorithms, J. Comp. Chem. 29 (2008) 839–845.

[28] S.W. Ng, Crystal structures of 2-[bis(triphenylphosphine)silver(I)]benzisothiazol-3 (2H)-one 1,1-dioxide and 2-[bis(triphenylphosphine)silver(I)]-4,5-dimethylisothiazol-3(2H)-one 1,1-dioxide ethanol, Z. Kristallogr. Mat. 210 (3) (1995) 206–209.

[29] F.A. Cotton, X. Feng, M. Matusz, R. Poli, Experimental and theoretical studies of the copper (I) and silver (I) dinuclear N, N'-di-p-tolylformamidinato complexes, J. Am. Chem. Soc. 110 (21) (1988) 7077–7083.

[30] W. Hsu, X.K. Yang, P.M. Chhetri, S.J. Lin, Y.S. Li, T.R. Chen, J.D. Chen, Au (I) and Ag (I) formamidinate tetranuclear complexes and coordination polymers: synthesis, structures and luminescent properties, Inorg. Chim. Acta 482 (2018) 785–790.

[31] S. Muthu, J.H. Yip, J.J. Vittal, Coordination networks of Ag (I) and N, N'-bis (3-pyridinecarboxamide)-1,6-hexane: structures and anion exchange, J. Chem. Soc. Dalton Trans. 24 (2002) 4561–4568.

[32] V.T. Yilmaz, S. Hamamci, W.T. Harrison, C. Thöne, Di-and tetranuclear silver (I)-saccharinate complexes with 2-pyridineethanol and 2-pyridinepropanol: syntheses, crystal structures, spectroscopic and thermal analyses of [Ag2(sac)2(pyet)2] and [Ag4(sac)4(pypr)2], Polyhedron 24 (5) (2005) 693–699.

[33] V.T. Yilmaz, S. Hamamci, O. Büyükgüngör, One-dimensional silver coordination polymers generated from saccharinate, piperazine and N, N'-bis (2-hydroxyethyl) piperazine, Polyhedron 27 (6) (2008) 1761–1766.

[34] V.T. Yilmaz, S. Hamamci, W.T. Harrison, Synthesis, IR spectra, thermal analysis and crystal structure of a one-dimensional coordination polymer containing both three-and four-coordinate silver (I) centers bridged by both saccharinate and N-(2-hydroxyethyl) piperazine ligands, J. Mol. Struct. 734 (1–3) (2005) 191–195.

[35] S.M. Soliman, Molecular structure, spectroscopic properties, NLO and NBO analysis of 3, 4-Lutidine and [Ag(3,4-Lutidine)2NO3] complex, J. Mol. Struct. 1048 (2013) 308–320.

[36] F.L. Hirshfeld, Bonded-atom fragments for describing molecular charge densities, Theor. Chim. Acta 44 (2) (1977) 129–138.

[37] S.M. Soliman, J. Albering, M.A.M. Abu-Youssef, Structural analyses of two new highly distorted octahedral copper (II) complexes with quinoline-type ligands; Hirshfeld, AIM and NBO studies, Polyhedron 127 (2017) 36–50.

[38] M.A. Spackman, P.G. Byrom, A novel definition of a molecule in a crystal, Chem. Phys. Lett. 267 (3–4) (1997) 215–220.

[39] A. Parkin, G. Barr, W. Dong, C.J. Gilmore, D. Jayatilaka, J.J. McKinnon, M. A. Spackman, C.C. Wilson, Comparing entire crystal structures: structural genetic fingerprinting, CrystEngComm 9 (8) (2007) 648–652.

[40] S. Celik, M. Alp, S. Yurdakul, A combined experimental and theoretical study on vibrational spectra of 3-pyridyl methyl ketone, Spectrosc. Lett. 53 (4) (2020) 234–248.

[41] M.T. Bilkan, Ş. Yurdakul, Z. Demircioğlu, O. Büyükgüngör, Crystal structure, FT-IR, FT-Raman and DFT studies on a novel compound [C10H9N3]4AgNO3, J. Organomet. Chem. 805 (2016) 108–116.

[42] B. Morzyk-Ociepa, D. Michalska, Vibrational spectra of 1-methyluracilate complex with silver (I) and theoretical studies of the 1-MeU anion, Spectrochim. Acta A Mol. Biomol. Spectrosc. 59 (6) (2003) 1247–1254.

[43] I. Bytheway, M.W. Wong, The prediction of vibrational frequencies of inorganic molecules using density functional theory, Chem. Phys. Lett. 282 (3–4) (1998) 219–226.

[44] G. Gece, S. Bilgic, A theoretical study on the inhibition efficiencies of some amino acids as corrosion inhibitors of nickel, Corros. Sci. 52 (10) (2010) 3435–3443.

[45] Ş. Yurdakul, S. Badoğlu, Y. Güleşci, Experimental and theoretical study on free 5-nitroquinoline, 5-nitroisoquinoline, and their zinc (II) halide complexes, Spectrochim. Acta A Mol. Biomol. Spectrosc. 137 (2015) 945–956.

[46] N.L. John, S. Abraham, J. George, P. Karuppasamy, M. Senthilpandian, P. Ramasamy, G. Vinitha, Synthesis, structure, NBO, Hirshfeld surface, NMR, HOMO-LUMO, UV, photoluminescence, z scan, vibrational and thermal analysis of piperazinedi-ium tetrakis (μ2chloro)-diaqua-dichloro-di-cadmium single crystal, J. Mol. Struct. 1258 (2022), 132685.

[47] Y. Ruiz-Morales, HOMO− LUMO gap as an index of molecular size and structure for polycyclic aromatic hydrocarbons (PAHs) and asphaltenes: a theoretical study, J. Phys. Chem. A 106 (46) (2002) 11283–11308.

[48] B. Sureshkumar, Y.S. Mary, C.Y. Panicker, K.S. Resmi, S. Suma, S. Armaković, S. J. Armaković, C. Van Alsenoy, Spectroscopic analysis of 8-hydroxyquinoline-5-

sulphonic acid and investigation of its reactive properties by DFT and molecular dynamics simulations, J. Mol. Struct. 1150 (2017) 540–552.

[49] S. Hosna, D.E. Janzen, Y.S. Mary, K.S. Resmi, R. Thomas, R. Mohamed, S. Wajda, Molecular structure, spectroscopic, dielectric and thermal study, nonlinear optical properties, natural bond orbital, HOMO-LUMO and molecular docking analysis of $(C_6Cl_2O_4)(C_{10}H_{14}N_2F)_2 \cdot 2H_2O$, Spectrochim. Acta A Mol. Biomol. Spectrosc. 204 (2018) 328–339.

[50] D. Majumdar, S. Das, R. Thomas, Z. Ullah, S.S. Sreejith, D. Das, P. Shukla, K. Bankura, D. Mishra, Syntheses, X-ray crystal structures of two new Zn (II)-dicyanamide complexes derived from H_2vanen-type compartmental ligands: investigation of thermal, photoluminescence, *in vitro* cytotoxic effect and DFT-TDDFT studies, Inorg. Chim. Acta 492 (2019) 221–234.

[51] I. Mantasha, M. Shahid, M. Kumar, A. Ansari, M.N. Akhtar, M.A. AlDamen, Y. Song, M. Ahmad, I.M. Khan, Exploring solvent dependent catecholase activity in transition metal complexes: an experimental and theoretical approach, New J. Chem. 44 (4) (2020) 1371–1388.

[52] C. Zhao, K.R. Ma, Y. Zhang, Y.H. Kan, R.Q. Li, H.Y. Hu, Structural, spectral and magnetic studies of two Co (II)-N-heterocyclic diphosphonates based on multinuclear units, Spectrochim. Acta A Mol. Biomol. Spectrosc. 153 (2016) 171–177.

[53] S. Sanotra, R. Gupta, U. Gupta, Y. Khajuria, H.N. Sheikh, Synthesis, crystal structure, photoluminescence, and DFT studies of bis (1, 10-phenanthroline) di (κ^2OO′ nitrato) cadmium (II)[C(*phen*)$_2$(NO$_3$)$_2$], Spectrochim. Acta A Mol. Biomol. Spectrosc. 129 (2014) 392–399.

[54] K.M. Langner, W.L. Beker, E. Dyguda-Kazimierowicz, W.A. Sokalski, Tracking molecular charge distribution along reaction paths with atomic multipole moments, Struct. Chem. 27 (2) (2016) 429–438.

[55] W. Yang, W.J. Mortier, The use of global and local molecular parameters for the analysis of the gas-phase basicity of amines, J. Am. Chem. Soc. 108 (19) (1986) 5708–5711.

[56] L.M. Rodríguez-Valdez, A. Martínez-Villafañe, D. Glossman-Mitnik, Computational simulation of the molecular structure and properties of heterocyclic organic compounds with possible corrosion inhibition properties, J. Mol. Struct. Theochem. 713 (1–3) (2005) 65–70.

[57] P. Devi, S. Fatma, A. Bishnoi, K. Srivastava, S. Shukla, R. Kumar, Synthesis, spectroscopic and DFT studies of novel 4-(morpholinomethyl)-5-oxo-1-phenylpyrrolidine-3-carboxylic acid, J. Mol. Struct. 1157 (2018) 551–559.

[58] R. Afzali, M. Vakili, E. Boluri, S.F. Tayyari, A.R. Nekoei, M. Hakimi-Tabar, V. Darugar, Structure, isomerism, and vibrational assignment of aluminumtrifluoroacetylacetonate. an experimental and theoretical study, Spectrochim. Acta A Mol. Biomol. Spectrosc. 190 (2018) 15–22.

[59] M. Rocha, A. Di Santo, J.M. Arias, D.M. Gil, A.B. Altabef, Ab-initio and DFT calculations on molecular structure, NBO, HOMO–LUMO study and a new vibrational analysis of 4-(Dimethylamino) Benzaldehyde, Spectrochim. Acta A Mol. Biomol. Spectrosc. 136 (2015) 635–643.

[60] S. Kecel-Gunduz, B. Bicak, S. Celik, S. Akyuz, A.E. Ozel, Structural and spectroscopic investigation on antioxidant dipeptide, L-Methionyl-L-Serine: a combined experimental and DFT study, J. Mol. Struct. 1137 (2017) 756–770.

[61] R.M. Asath, S. Premkumar, T. Mathavan, A.M.F. Benial, Vibrational spectroscopic, molecular docking and quantum chemical studies on 6-aminonicotinamide, J. Mol. Struct. 1134 (2017) 143–156.